Carbohydrate Polymers 121 (2015) 115–121

Contents lists available at ScienceDirect

Carbohydrate Polymers

journal homepage: www.elsevier.com/locate/carbpol

Self-assemblied nanocomplexes based on biomimetic amphiphilic chitosan derivatives for protein delivery

Minming Wu, Hongwei Dong, Kai Guo, Rong Zeng*, Mei Tu, Jianhao Zhao

Department of Materials Science and Engineering, College of Science and Engineering, Jinan University, Guangzhou 510632, PR China

ARTICLE INFO

Article history:
Received 9 September 2014
Received in revised form
10 December 2014
Accepted 12 December 2014
Available online 2 January 2015

Keywords:
Biomimetic
Chitosan
Self-assembly
Nanocomplexes
Protein delivery

ABSTRACT

A bio-inspired nanocarrier was developed for protein delivery based on biodegradable amphiphilic chitosan derivative (DCA–PCCs) with hydrophilic cell membrane mimic phosphorylcholine (PC) and hydrophobic deoxycholic acid (DCA) moieties, which was synthesized *via* the combination of Atherton–Todd reaction and carbodiimide coupling reaction. Using bovine serum albumin (BSA) as model protein, it was found that DCA–PCCs with suitable degree of substitution of PC and DCA moieties can load proteins by forming nanocomplexes *via* a solvent evaporation method. The physicochemical characteristics of BSA/DCA–PCCs nanocomplexes were investigated by Zetasizer, atomic force microscopy (AFM) and Fourier-transform infrared (FT-IR) spectroscopy. *In vitro* biological evaluation revealed BSA/DCA–PCCs nanocomplexes as blank DCA–PCCs nanoparticles had excellent cytocompatibility and hemocompatibility mainly due to the presence of cell membrane mimic phosphorylcholine. BSA release results suggested BSA/DCA–PCCs nanocomplexes showed a sustained release behavior following first order exponential decay kinetics. The results indicated DCA–PCCs provided a promising approach for effectively delivering therapeutic proteins.

1. Introduction

Bio-inspired nanosystems have been widely investigated for delivering therapeutic and/or diagnostic agents such as DNA, RNA, peptides, chemical drugs, or contrast/imaging agents, since they can protect sensitive cargo, pass through physiological barriers, avoid the clearance by the body's natural defence mechanisms, and target to specific sites *in vivo* by mimicking natural delivery vehicles (Balmert & Little, 2012; Jayakumar et al., 2010; Muzzarelli, 2010; Yoo, Irvine, Discher, & Mitragostri, 2011). Among them, cell membrane mimic zwitterionic phosphorylcholine (PC) based nanosystems have attracted much interest due to their excellent hemocompatibility and protein-resistant property (Matsuno & Ishihara, 2011), which provided an alternative strategy for suppressing the non-specific interactions of nanosystems with biological components to avoid the undesired biological response, except the conventional poly(ethylene glycol) (PEG)ylation. More interestingly, PC-based nanosystems could enter living cells through fusogenic interaction with the plasma membrane (Son et al., 2011) and be selectively uptaked by different types of cancer cells than normal cells (Zhou, Liu, & Ji, 2012). Considering some unfavorable biological response related to PEGylation reported recently, such as the accelerated blood clearance (ABC) phenomenon (Shiraishi et al., 2013) and inhibitation of cell uptake (Hatakeyama, Akita, & Harashima, 2011), PC-based nanosystems showed great advantage over PEGylated nanosystems. However, most of PC-based nanosystyems reported were based on non-biodegradable 2-methacryloyloxyethyl phosphorylcholine (MPC) copolymers (Salvage et al., 2005), which would greatly restrict their pharmaceutical and biomedical application *in vivo*, and few reports have been published on protein delivery application.

Pharmaceutical proteins with high activity and specificity represent a promising approach for treating a variety of diseases, but poor stability and low bioavailability limit their application. Thus, safe and efficient protein delivery systems are in great demand (Salmaso & Caliceti, 2013). As far as we know, biodegradable chitosan-based delivery nanosystems have shown great potency in therapeutic peptides and proteins delivery, however there still existed some hurdles such as poor efficacy and possible long-term toxicity need to be cleared for their clinical application (Amidi, Mastrobattista, Jiskoot, & Hennink, 2010; Koppolu et al., 2014; Li et al., 2010). In our previous work, we have successfully synthesized biomimetic PC–chitosan conjugates (PCCs) with different degree of substitution (DS) *via* a phosphoramide linkage between glucosamine and PC through Atherton–Todd reaction and subsequent

* Corresponding author. Tel.: +86 20 85223271; fax: +86 20 85223271.
E-mail address: tzengronga@jnu.edu.cn (R. Zeng).

http://dx.doi.org/10.1016/j.carbpol.2014.12.049
0144-8617/

hydrolysis under the mild conditions, which can self-assemble to form PC-covered spherical micelles (Zeng et al., 2012), and revealed that PC can suppress the non-specific protein interactions between PCCs and protein (Wang, Zeng, Tu, & Zhao, 2012), which benefited the biocompatibility of PCCs-based nanocarriers but limited their protein loading properties.

In this work, we report a facile approach to construct bio-inspired biodegradable nanocomplexes for protein delivery based on the self-assembly of amphiphilic chitosan derivatives with hydrophilic PC and hydrophobic deoxycholic acid (DCA) moieties. Firstly, amphiphilic deoxycholic acid–phosphorylcholine–chitosan conjugates (DCA–PCCs) were prepared by further introducing DCA to PCCs, and its hydrophilicity/hydrophobicity balance was optimized by controlling both DS values of PC and DCA. Bovine serum albumin (BSA) was used as a model protein to investigate protein loading and releasing capacity. Biocompatibility assay results implied that amphiphilic biomimetic DCA–PCCs may be an attractive candidate for protein delivery.

2. Materials and methods

2.1. Materials

Chitosan (low molecular weight, Brookfield viscosity: 20 cps) was purchased from Sigma–Aldrich, then treated with 40% NaOH at 110 °C for 1.5 h three times to reach 100% deacetylation degree (confirmed by no signal associated to acetyl groups in ^{1}H NMR spectra) and purified before using. Diphenyl phosphite was also purchased from Sigma–Aldrich. Choline chloride was obtained from Acros. *N*-Hydroxysuccinimide (NHS), 1-ethyl-3-(3-dimethylaminopropyl) carbodiimide hydrochloride (EDAC) and deoxycholic acid (DCA) were purchased from Aladdin Reagent Company (China). Bovine serum albumin (BSA) was purchased from Beijing Dingguo Biotechnology Co., Ltd. Other chemicals and solvents were of analytical grade.

2.2. Methods

2.2.1. Synthesis and characterization of amphiphilic chitosan derivatives

DCA–PCCs were synthesized according to the procedure based on the Atherton–Todd reaction for introducing PC and subsequent carbodiimide coupling reaction for coupling DCA to the amino groups of chitosan, and all experiments involving water-sensitive compounds were conducted under dry conditions. Firstly, PCCs were synthesized according to our previous work (Zeng et al., 2012). 726 mg (5.2 mmol) of choline chloride was added to 0.475 mL (2.5 mmol) of diphenyl phosphite in 10 mL of freshly distilled pyridine/DMSO (1:10) at room temperature, then stirred for 2 h. The crude product of dicholinyl H-phosphonate dichloride was obtained after the solvent was evaporated, dissolved in 10 mL of 2-propanol, then slowly added dropwise to 6-*O*-trityl chitosan obtained according to Nishimura's method (Nishimura, Kohgo, Kurita, & Kuzuhara, 1991) (200 mg, 0.50 mmol of free NH_2) in a mixed solution of dimethylacetamide (DMA, 10 mL), triethylamine [1.05 mL (7.5 mmol)], and tetrachloromethane [0.475 mL (5.0 mmol)] in ice-water bath. After stirring overnight, the resulting solution was evaporated to dryness, 10 mL of formic acid was added to the residue, stirred for 1 h, then formic acid was removed by rotary evaporation. The residue was dissolved in 10 mL of 0.1 mol/L NaOH and stirred for 2 h, then centrifuged. The supernatant was dialyzed with distilled water for 3 days and lyophilized to provide the PCCs (113.2 mg). Then, PCCs (100 mg) was dissolved in 1% (w/v) acetic acid solution (20 mL), followed by the addition of DCA at 2.0 mol/mol glucosamine residue of chitosan after activation by EDAC and NHS (DCA:EDAC:NHS = 1:1.5:1.2, mol/mol) in 50 mL methanol. The solution was stirred at room temperature for 48 h, then dialyzed against methanol for 1 day and then distilled water for 3 days. The DCA–PCCs product (96.5 mg) was obtained by lyophilization.

^{1}H and ^{31}P NMR spectra were recorded in D_2O at 400 MHz using a Bruker UX-400 NMR spectrometer (Germany). The degree of substitution (DS, defined as the number of PC per 100 glucosamine residues) of PC moiety was calculated by the amount ratio of H of $-N^+(CH_3)_3$ (from PC) to H1 (from glucosamine units of GlcN and GlcN-PC). The DS of DCA (defined as the number of DCA per 100 glucosamine residues) was determined spectrophotometrically using the method described by Wang et al. (2011). Briefly, the DCA–PCCs sample (4–10 mg) was accurately weighed in an ampoule and dissolved in 0.5 mL DMSO, then 0.5 mL of 60% acetic acid solution and 9.0 mL of a mixture H_2O/H_2SO_4 (65/50, v/v) were added. After homogenization, the content of the ampoule was kept at 70 °C for 30 min then cooled to room temperature. The absorbance at 378 nm was measured against a blank containing the same components but without polymer. A series of gradient DCA standard solution were also prepared to make the calibration curve following the above procedure. The DS of DCA was calculated according to Eq. (1):

$$\text{DS}\ \ (\%) = \frac{c/M_{\text{DCA}}}{(m-c)/M_{\text{PCCs}}} \times 100\% \quad (1)$$

where c (g) is the content of the DCA determined by the corresponding calibration curve, m (g) is the amount of the DCA–PCCs used in measurement, M_{DCA} is the molecular mass of DCA, M_{PCCs} is the molecular mass of PCCs units.

2.2.2. Preparation and characterization of BSA/DCA–PCCs nanocomplexes

BSA was loaded into DCA–PCCs carriers by a solvent evaporation method (Li et al., 2010). Briefly, DCA–PCCs (10 mg) was dissolved in distilled water (1 mL), diluted with ethanol (4 mL), and mixed with 1 mL of BSA solution in distilled water (1 mg/mL). The solvents were then evaporated at 40 °C using a rotary evaporator, to obtain a thin BSA/DCA–PCCs film. After addition of 10 mL of distilled water, the solution was gently stirred for 10 min and filtered through a 0.45 μm filter (Millipore), and subsequently lyophilized after centrifugation to obtain BSA/DCA–PCCs nanocomplexes. The blank DCA–PCCs nanoparticles were obtained for comparison by the solvent evaporation method at the same conditions. The morphology, size and zeta potential of BSA/DCA–PCCs nanocomplexes were measured by AFM (Bioscope catalyst) and Zetasizer (Malvern). The interactions between BSA and DCA–DCA–PCCs were investigated by FT-IR spectroscopy (Bruker, Equinox-55, Germany) in KBr. The BSA loading capacity (LC, amount of BSA loaded/mass of BSA/DCA–PCCs nanocomplexes) and loading efficiency (LE, amount of BSA loaded/total amount of BSA in feeding) were determined by BCA assay, since no signal from blank DCA–PCCs nanoparticles was detected using BCA method.

2.2.3. Cytotoxicity assay

The cytotoxicity of blank DCA–PCCs nanoparticles and BSA/DCA–PCCs nanocomplexes was monitored using NIH/3T3 mouse embryonic fibroblasts by MTT assay based on the reduction of MTT by mitochondria in viable cells to water-insoluble formazan, as well as LDH assay based on measuring the release of the cytosolic enzyme lactate dehydrogenase due to cell membrane damage (Fischer, Li, Ahlemeyer, Krieglstein, & Kissel, 2003).

In MTT assay, NIH/3T3 mouse embryonic fibroblasts were treated with two sample nanoparticles stock solutions varying from 0.25 to 2.0 mg/mL for 1 day. 1% Triton X-100 was used as a positive control, experiment was done using a MTT cytotoxicity assay kit (Vybrant® MTT Cell Proliferation Assay Kit) following the

instruction of manufacturer's manual. The relative cell viability (%) related to control wells containing cell culture medium without sample was calculated by $[A]_{test}/[A]_{control} \times 100$. All experiments were repeated in triplicate.

In LDH assay, the amount of LDH leaked from NIH/3T3 mouse embryonic fibroblast cells after 4 h incubation with serial dilutions of blank DCA–PCCs nanoparticles or BSA/DCA–PCCs nanocomplexes (from 0.25 to 2.0 mg/mL) was measured using a LDH cytotoxicity assay kit (Thermo Fisher Pierce), according to the manufacturer's manual. 0.1% Triton X-100 was used as a positive control. All samples were run in triplicate.

2.2.4. Hemolysis assay and RBCs morphology study

Blood sampling procedures were approved by the ethics committee of Jinan University. Hemolytic activity of blank DCA–PCCs nanoparticles and BSA/DCA–PCCs nanocomplexes was evaluated by measuring hemoglobin release from rabbit red blood cells (RBCs). Hemolysis assay was conducted as described by Oda, Kanaoka, Sato, Aoshima, and Kuroda (2011), HEPES buffer was used as negative hemolysis control and Triton X-100 (10 μL, 1%, v/v) as positive hemolysis control. The percentage of hemolysis was calculated by Eq. (2):

$$H(\%) = \frac{A - A_0}{A_{100} - A_0} \times 100\% \quad (2)$$

where A is the absorbance of the test sample, A_0 is the absorbance of the negative control, A_{100} is the absorbance of the positive control.

RBCs morphology study was conducted as described in our previous job (Wu et al., 2014), normal saline was used as negative control. The fixed RBCs were coated with gold and examined by scanning electron microscope (SEM, JEOL JC60X).

2.2.5. In vitro release of BSA from BSA/DCA–PCCs nanocomplexes study

2 mg BSA/DCA–PCCs nanocomplexes were dispersed in 5 mL PBS (pH 7.4) incubated on a shaking water-bath at 37 °C, 100 rpm, and sampled at predetermined intervals with adding an equal volume of buffer solution to maintain a constant volume of releasing medium. After ultra centrifugation at 20 000 rpm for 30 min, the amount of released BSA in the supernatant was determined by BCA assay. Each experiment was repeated in triplicate.

3. Result and discussion

3.1. Synthesis of DCA–PCCs

Amphiphilic chitosan derivative DCA–PCCs was synthesized according to the procedure as shown in Scheme 1. It should be noted that both DS values of hydrophilic PC and hydrophobic DCA moieties of DCA–PCCs could be adjusted by changing the reactant ratio in the Atherton–Todd reaction and carbodiimide coupling reaction, respectively, which would greatly affect the hydrophilicity/hydrophobicity balance of DCA–PCCs, and subsequent their interactions and self-assembly behaviors with proteins. In this work, DCA–PCCs with DS (DCA) = 3.0% and DS (PC) = 42% was prepared for protein delivery. The DS of PC moiety of DCA–PCCs was calculated by the amount ratio of H of $-N^+(CH_3)_3$ (from PC) to H1 (from glucosamine units of GlcN and GlcN-PC) based on the ^{1}H NMR spectra, while the DS of DCA moiety of DCA–PCCs was determined by a spectrophotometrical method because the signals from DCA protons could not be exactly quantified in the ^{1}H NMR spectra.

Fig. 1 showed the ^{1}H and ^{31}P NMR spectra of DCA–PCCs. As shown Fig. 1a, the signals at 4.67 ppm and 2.98 ppm were attributed to H1 and H2, and 3.50–3.71 ppm for H3, H4, H5, and H6 of chitosan, respectively. The relevant signals of PC characteristic peaks appeared at 3.14 ppm and 4.21 ppm, which were assigned to hydrogen protons of $N^+(C\underline{H}_3)_3$ and the methylene protons of $N^+(CH_3)_3—CH_2—C\underline{H}_2—$, respectively, indicating the successful coupling PC to chitosan backbone. Meanwhile, the proton signal of $N^+CH_2—$ of PC overlapped with the H3–H6 signals at 3.50–3.71 ppm of chitosan. Moreover, the characteristic signals of DCA appeared in the range of 0.68–1.12 ppm (Wang et al., 2011). The aforementioned ^{1}H NMR spectra results proved the successful synthesis of DCA–PCCs. Additionally, the single peak at 6.00 ppm in the ^{31}P NMR spectra of DCA–PCCs further confirmed the formation of phosphoramide linkage between glucosamine and PC as shown in Fig. 1b.

3.2. Formation of blank DCA–PCCs nanoparticles and BSA/DCA–PCCs nanocomplexes

It has been reported that amphiphilic copolymers can self-assemble to form nanocomplexes with protein drugs by physical specific or unspecific interactions to increase the stability and bioavailability of proteins (Li et al., 2010; Salmaso & Caliceti, 2013). We have synthesized a series of amphiphilic chitosan derivatives DCA–PCCs with the same DS (PC) value (42%) but different DS (DCA) value for loading BSA by a solvent evaporation method. It was found that DCA–PCCs with lower DS (DCA) value (*e.g.* 1.9%) like PCCs could not form nanocomplexes with BSA probably due to the weak hydrophobic interaction between DCA moiety and BSA and the repulsive force between PC moiety and BSA, according to the results of Zetasizer, AFM and BCA assay. In this work, BSA was successfully loaded into DCA–PCCs with DS (DCA) = 3.0% and DS (PC) = 42% by forming nanocomplexes. Actually, the formation of BSA/DCA–PCCs nanocomplexes by self-assembly in ethanol/water was mainly due to not only the hydrophilicity/hydrophobicity balance of DCA–PCCs itself, but also the balance of interactions between BSA and DCA–PCCs. The higher DS of PC would lead to the higher hydrophilicity of DCA–PCCs, but lower the BSA loading due to the protein-resistant property of PC, while the increase of DS (DCA) of DCA–PCCs would increase the hydrophobicity of DCA–PCCs and its hydrophobic interaction with BSA, which was beneficial to the BSA loading. Additionally, DCA–PCCs with lower DS (PC) and higher DS (DCA) would show poor water solubility and poor hemocompatibility. Thus only DCA–PCCs with suitable degree of substitution of PC and DCA moieties can form spherical nanocomplexes loaded BSA with high loading efficiency by self-assembly. The LC and LE of BSA in nanocomplexes were 15.6% and 80.5%, respectively, determined by BCA assay, which were similar to the results of BSA-loaded 5β-cholanic acid conjugated glycol chitosan nanocomplexes (Li et al., 2010).

Fig. 2 showed that the size and morphology of BSA/DCA–PCCs nanocomplexes. The mean hydrodynamic diameter of BSA/DCA–PCCs nanocomplexes was 213.0 ± 2.8 nm with PDI (polydispersity index) = 0.195 measured using DLS technique, and their zeta potential was 13.4 ± 0.39 eV, while the blank DCA–PCCs nanoparticles with hydrophobic DCA core and hydrophilic PC shell prepared using solvent evaporation method at the same conditions showed larger size and size distribution (mean hydrodynamic diameter = 285.3 ± 4.7 nm, PDI = 0.253), and lower surface potential (zeta potential = 5.49 ± 0.43 eV). It seems that the interactions between DCA–PCCs and BSA caused BSA/DCA–PCCs nanocomplexes smaller than blank DCA–PCCs self-assemblied nanoparticles, but pushed more residue amino groups of chitosan to the shell, leading a higher zeta potential. However, the zeta potential of nanocomplexes was still much smaller than that of pure chitosan nanoparticles, about +35 mV (Brunel et al., 2010), probably due to the existence of electrically neutral zwitterionic PC groups in the surface, which was advantageous to prolong the circulation time of nanocomplexes in the bloodstream. AFM observation (Fig. 2b) confirmed that BSA and DCA–PCCs can

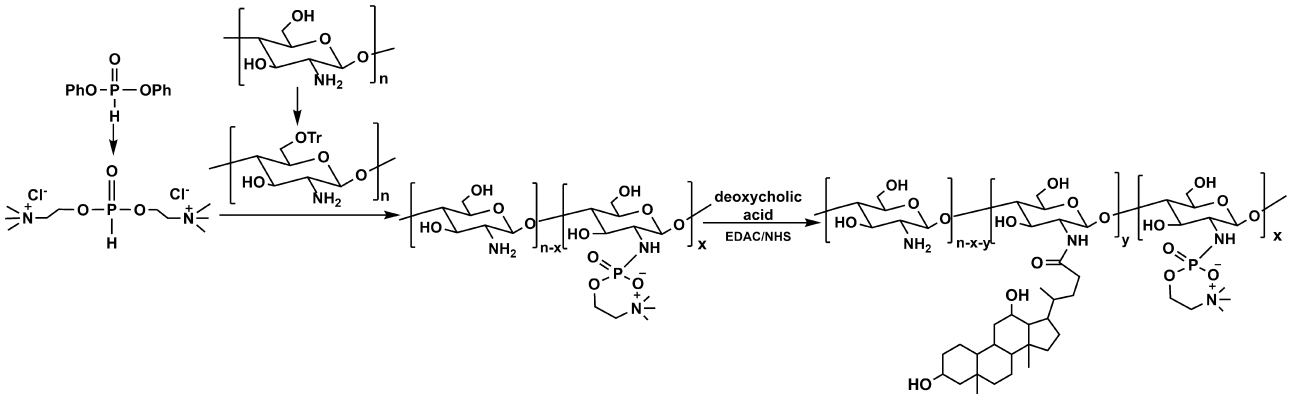

Scheme 1. Synthesis route of DCA–PCCs.

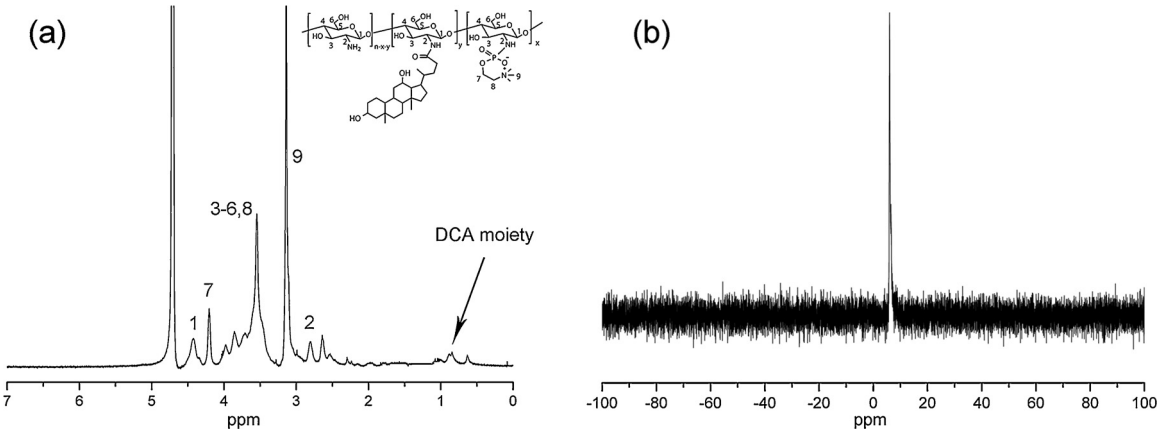

Fig. 1. ^{1}H NMR and ^{31}P NMR spectra of DCA–PCCs.

self-assemble to form spherical nanocomplexes with diameter about 150 nm in the dry state.

FT-IR spectroscopy can be used to explore the secondary structure and conformation change of proteins, as well as the interactions between protein and materials (Falini et al., 2006; Li, Tian, Liu, & Zhao, 2009; Murayama & Tomida, 2004; Swain & Sarkar, 2013). Fig. 3 depicted the FTIR spectra of lyophilized BSA, blank DCA–PCCs nanoparticles and BSA/DCA–PCCs nanocomplexes. The spectrum of pure BSA showed a broad N—H stretching vibration peak between 3300 and 3500 cm^{-1}, weak —CH_2 asymmetric and symmetric stretching at 2959 and 2874 cm^{-1}, as well as C=O stretching of amide-I at 1655 cm^{-1} and N—H bending of amide-II at 1543 cm^{-1}, which were in good agreement with the literature data (Falini et al., 2006). For the blank DCA–PCCs nanoparticles spectrum, the characteristic peaks appeared at 3300–3500 cm^{-1} represented the stretching vibration of —NH_2 and —OH groups, at 2968 and 2864 cm^{-1} ascribed to —CH_2 asymmetric and symmetric stretching, at 1644 cm^{-1} attributed to carbonyl stretching (amide I band), and at 1529 cm^{-1} assigned to N—H bending (amide-II). From the FTIR spectrum of the BSA/DCA–PCCs nanocomplexes, it was observed that —CH_2 asymmetric and symmetric stretching shifted to 2931 cm^{-1} and 2857 cm^{-1}, respectively, carbonyl stretching (amide I band) shifted to 1640 cm^{-1}, and N—H bending (amide II) weakened and shifted to 1555 cm^{-1}. The results clearly confirmed that BSA can form nanocomplexes with DCA–PCCs mainly by their hydrophobic and electrostatic interactions (Falini et al., 2006; Li

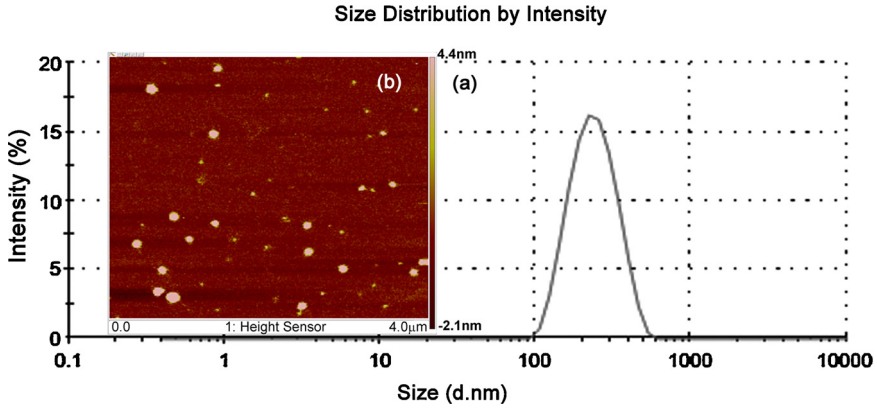

Fig. 2. (a) Size distribution and (b) AFM images of BSA/DCA–PCCs nanocomplexes.

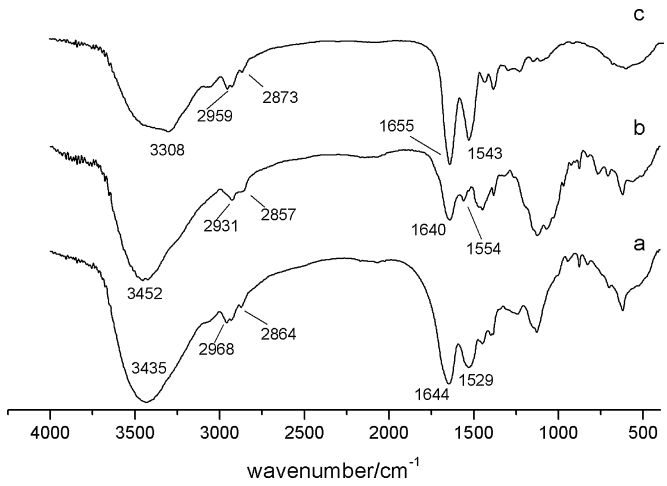

Fig. 3. FTIR spectra of (a) blank DCA–PCCs nanoparticles, (b) BSA/DCA–PCCs nanocomplexes, and (c) BSA.

et al., 2009; Swain & Sarkar, 2013), though the detailed analysis on the conformational change in the BSA structure can not be performed based on the FTIR spectra due to the overlap of amide I of BSA and DCA–PCCS.

3.3. Cytotoxicity of blank DCA–PCCs nanoparticles and BSA/DCA–PCCs nanocomplexes

The MTT assay was performed to assess the influence of BSA/DCA–PCCs nanocomplexes on the metabolic activity of NIH/3T3 fibroblasts in comparison with blank DCA–PCCs nanoparticles. Fig. 4 presented the cell viability of the two kinds of nanoparticles at various concentrations against NIH/3T3 cells after 24 h incubation. It could be found that both of them with positive surface charge showed a concentration dependent effect on the cytotoxicity, and all the NIH/3T3 cell viabilities in the presence of samples up to 2.0 mg/mL were above 80%. Actually, cationic macromolecules or nanoparticles usually affected the cytotoxicity of cells in a dose-dependent manner, which was also dependent on the density and arrangement of positive charges, though the mechanism was not yet fully understood. The cytotoxic effects may be caused by the interactions of polycations with negative charged

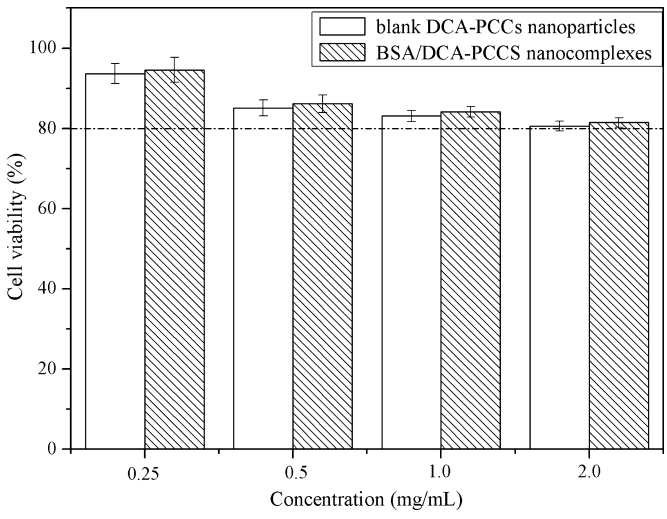

Fig. 4. Cell viability of blank DCA–PCCs nanoparticles and BSA/DCA–PCCs nanocomplexes at various concentrations against NIH/3T3 cells incubated for 24 h evaluated by the MTT assay. The values represent means ± SD ($n = 3$).

cell membranes, and/or by cellular uptake and subsequent activation of intracellular signal transduction pathways (Fischer et al., 2003). And according to ISO 10993-5, a cell viability lower than 70% in comparison to the blank control was regarded as cytotoxic. The blank DCA–PCCs nanoparticles and BSA/DCA–PCCs nanocomplexes up to 2.0 mg/mL were non-toxic, since both cell viabilities being above 70%.

To measure the cell membrane damaging effects of both blank DCA–PCCs nanoparticles and BSA/DCA–PCCs nanocomplexes, the extracellular concentration of LDH was quantified, which could be regarded as an indicator for early cytotoxicity. LDH release results from NIH/3T3 cells induced by blank DCA–PCCs nanoparticles and BSA/DCA–PCCs nanocomplexes at various concentrations after 4 h incubation showed that both of them up to 2.0 mg/mL did not induce LDH leakage larger than 10% which are regarded as non-cytotoxic effect level (Fischer et al., 2003), indicating that both of them up to 2.0 mg/mL did not induce significant damage of cell membranes (Bauer et al., 2012).

Both the MTT and LDH results suggested that blank DCA–PCCs nanoparticles and BSA/DCA–PCCs nanocomplexes exhibited low cytotoxicity probably due to the shielding effect of biomimetic hydrophilic PC groups in the surface.

3.4. Blood compatibility of blank DCA–PCCs nanoparticles and BSA/DCA–PCCs nanocomplexes

The effect of nanosystems on the erythrocytes is particularly important for their *in vivo* applications, which is usually measured for evaluating their blood compatibility (Bender et al., 2012). Fig. 5a showed the hemolytic activity induced by blank DCA–PCCs nanoparticles and BSA/DCA–PCCs nanocomplexes as a function of their concentrations. It was found that both of them also showed a dose-dependent effect on the erythrocytes. The hemolysis value was in the range of 1.0–2.0% below 1.0 mg/mL, indicating both nanocomparticles were non-hemolytic up to 1.0 mg/mL; while at 2.0 and 4.0 mg/mL were regarded as slightly hemolytic due to their hemolysis values in the range from 1.5% to 3.0%, below 5%, according to the ASTM standard F756-13.

Additionally, the effect of blank DCA–PCCs nanoparticles and BSA/DCA–PCCs nanocomplexes on the aggregation and morphology of RBCs was observed by SEM as shown in Fig. 5b–d. It could be seen that both nanoparticles at 1.0 mg/mL did not cause obvious RBCs aggregation and morphological change, most of RBCs kept their normally biconcave shape but few of them showed crenated shape with protrusions. Actually, the interaction between cationic amphiphilic copolymers and RBCs involved both the electrostatic attraction between the negative RBC surface charges and the positive charges of polycations, and the hydrophobic interaction between the hydrophobic groups of copolymers and the lipid bilayer of RBC membrane (Oda et al., 2011). Excessive interactions may result in the RBC aggregation and morphological change, and even lysis to release hemoglobin molecules. The above results suggested that both nanoparticles were quite non-hemolytic mainly owing to the existence of biomimetic hydrophilic PC groups in the surface, which can effectively suppress the damaging effects of nanocomplexes on RBCs.

3.5. Release of BSA from BSA/DCA–PCCs nanocomplexes

Fig. 6 showed the *in vitro* release profile of BSA from BSA/DCA–PCCs nanocomplexes in physiological condition determined by BCA method. The BSA showed a biphasic release profile, which could be classified into two periods due to the complicated mechanisms for biodegradable polymeric delivery systems (Silva, Ducheyne, & Reis, 2007), including diffusion of BSA, degradation of DCA–PCCs, and dissociation of BSA/DCA–PCCs nanocomplexes. It

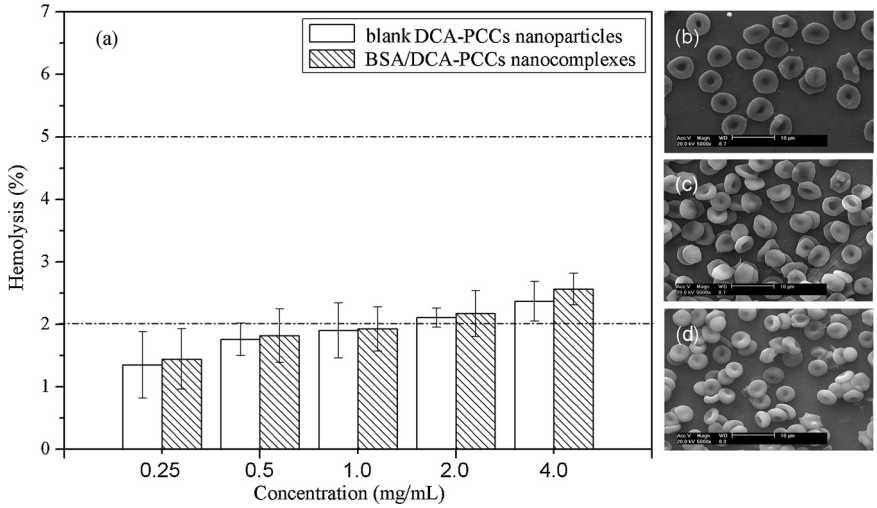

Fig. 5. (a) Percentages of hemolysis induced by blank DCA–PCCs nanoparticles and BSA/DCA–PCCs nanocomplexes as a function of their concentrations. The values represent means ± SD (n = 3), (b) SEM images of RBCs incubated with normal saline as negative control, (c) SEM images of RBCs incubated with blank DCA–PCCs nanoparticles at 1.0 mg/mL, and (d) SEM images of RBCs incubated with BSA/DCA–PCCs nanocomplexes at 1.0 mg/mL.

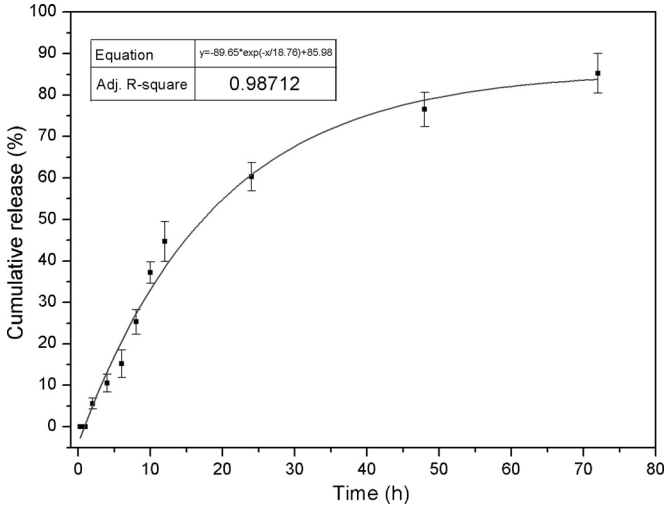

Fig. 6. Release profiles of BSA from BSA/DCA–PCCs nanocomplexes in physiological condition (pH 7.4, 37 °C), means ± SD (n = 3).

could be seen that about 45% BSA was rapidly released at first 12 h, followed by a slow release up to 72 h reaching a cumulative release of BSA close to 85%. And the results of BSA release studies were fitted with three common kinetic models (zero order kinetics, exponential first order kinetics and Higuchi kinetics equations) (Mehta & Jindal, 2013), it was found that the best agreement of the fitting has been achieved with the model of first order exponential decay equation (R^2 = 0.98712). The results indicated that BSA/DCA–PCCs nanocomplexes showed a sustained BSA release behavior.

4. Conclusion

Bio-inspired amphiphilic chitosan derivatives DCA–PCCs with hydrophilic phosphorylcholine and hydrophobic deoxycholic acid moieties were successfully synthesized *via* Atherton–Todd reaction and carbodiimide coupling reaction. It was found that DCA–PCCs with suitable degree of substitution of phosphorylcholine and deoxycholic acid moieties can form spherical nanocomplexes loaded BSA with high loading efficiency by self-assembly. The cytotoxicity and hemocompatibility assays confirmed that both blank DCA–PCCs nanoparticles and BSA/DCA–PCCs nanocomplexes showed excellent biocompatibility due to the presence of cell membrane mimic phosphorylcholine. *In vitro* release data revealed that BSA/DCA–PCCs nanocomplexes provided a prolonged release of BSA following first order exponential decay kinetics. It was supposed that biomimetic amphiphilic DCA–PCCs may be a promising carrier for protein delivery.

Acknowledgments

The authors would like to acknowledge financial support from the National Natural Science Foundation of China (Grant No. 31040027 and No. 31370974) and Research Development and Innovation Fund of Jinan University (No. 21611410).

References

Amidi, M., Mastrobattista, E., Jiskoot, W., & Hennink, W. E. (2010). Chitosan-based delivery systems for protein therapeutics and antigens. *Advanced Drug Delivery Reviews*, *62*, 59–82.

ASTM F756-13. (2013). *Standard practice for assessment of hemolytic properties of materials*. ASTM International.

Balmert, S. C., & Little, S. R. (2012). Biomimetic delivery with micro- and nanoparticles. *Advanced Materials*, *24*, 2757–2778.

Bauer, M., Lautenschaeger, C., Kempe, K., Tauhardt, L., Schubert, U. S., & Fischer, D. (2012). Poly(2-ethyl-2-oxazoline) as alternative for the stealth polymer poly(ethylene glycol): Comparison of in vitro cytotoxicity and hemocompatibility. *Macromolecular Bioscience*, *12*, 986–998.

Bender, E. A., Adorne, M. D., Colomé, L. M., Abdalla, D. S. P., Guterres, S. S., & Pohlmann, A. R. (2012). Hemocompatibility of poly(ε-caprolactone) lipid-core nanocapsules stabilized with polysorbate 80-lecithin and uncoated or coated with chitosan. *International Journal of Pharmaceutics*, *426*, 271–279.

Brunel, F., Véron, L., David, L., Domard, A., Verrier, B., & Delair, T. (2010). Self-assemblies on chitosan nanohydrogels. *Macromolecular Bioscience*, *10*, 424–432.

Falini, G., Foresti, E., Lesci, I. G., Bruno, L., Piera, S., & Norberto, R. (2006). Interaction of bovine serum albumin with chrysotile: Spectroscopic and morphological studies. *Chemisty – A European Journal*, *12*, 1968–1974.

Fischer, D., Li, Y. X., Ahlemeyer, B., Krieglstein, J., & Kissel, T. (2003). In vitro cytotoxicity testing of polycations: Influence of polymer structure on cell viability and hemolysis. *Biomaterials*, *24*, 1121–1131.

Hatakeyama, H., Akita, H., & Harashima, H. (2011). A multifunctional envelope type nano device (MEND) for gene delivery to tumours based on the EPR effect: A strategy for overcoming the PEG dilemma. *Advanced Drug Delivery Reviews*, *63*, 152–160.

ISO 10993-5. (2009). *Biological evaluation of medical devices. Part 5: Tests for in vitro cytotoxicity*. International Organization for Standardization.

Jayakumar, R., Chennazhi, K. P., Muzzarelli, R. A. A., Tamura, H., Nair, S. V., & Selvamurugan, N. (2010). Chitosan conjugated DNA nanoparticles in gene therapy. *Carbohydrate Polymers*, *79*, 1–8.

Koppolu, B. P., Smith, S. G., Ravindranathan, S., Jayanthi, S., Kumar, T. K. S., & Zaharoff, D. A. (2014). Controlling chitosan-based encapsulation for protein and vaccine delivery. *Biomaterials*, *35*, 4382–4389.

Li, F., Tian, F., Liu, C. J., & Zhao, Y. L. (2009). Preparation and characterization of improved microspheres containing bovine serum albumin. *Journal of Applied Polymer Science*, *114*, 818–825.

Li, T., Longabardi, L., Granero-Molto, F., Myers, T. J., Yan, Y., & Spagnoli, A. (2010). Use of glycol chitosan modified by 5β-cholanic acid nanoparticles for the sustained release of proteins during murine embryonic limb skeletogenesis. *Journal of Controlled Release*, *144*, 101–108.

Matsuno, R., & Ishihara, K. (2011). Integrated functional nanocolloids covered with artificial cell membranes for biomedical applications. *Nanotoday*, *6*, 61–74.

Mehta, S. K., & Jindal, N. (2013). Mixed micelles of lecithin–tyloxapol as pharmaceutical nanocarriers for anti-tubercular drug delivery. *Colloids and Surfaces B*, *110*, 419–425.

Murayama, K., & Tomida, M. (2004). Heat-induced secondary structure and conformation change of bovine serum albumin investigated by Fourier transform infrared spectroscopy. *Biochemistry*, *43*, 11526–11532.

Muzzarelli, R. A. A. (2010). Chitosans: New vectors for gene therapy. In R. Ito, & Y. Matsuo (Eds.), *Handbook of carbohydrate polymers: Development, properties and applications* (pp. 583–604). Hauppauge, NY: Nova Science Publishers, Inc.

Nishimura, S., Kohgo, O., Kurita, K., & Kuzuhara, H. (1991). Chemospecific manipulations of a rigid polysaccharide: Syntheses of novel chitosan derivatives with excellent solubility in common organic solvents by regioselective chemical modifications. *Macromolecules*, *24*, 4745–4748.

Oda, Y., Kanaoka, S., Sato, T., Aoshima, S., & Kuroda, K. (2011). Block versus random amphiphilic copolymers as antibacterial agents. *Biomacromolecules*, *12*, 3581–3591.

Salmaso, S., & Caliceti, P. (2013). Self assembling nanocomposites for protein delivery: Supramolecular interactions of soluble polymers with protein drugs. *International Journal of Pharmaceutics*, *440*, 111–123.

Salvage, J. P., Rose, S. F., Phillips, G. J., Hanlon, G. W., Lloyd, A. W., Ma, I. Y., et al. (2005). Novel biocompatible phosphorylcholine-based self-assembled nanoparticles for drug delivery. *Journal of Controlled Release*, *104*, 259–270.

Shiraishi, K., Hamano, M., Ma, H., Kawano, K., Maitani, Y., Aoshi, T., et al. (2013). Hydrophobic blocks of PEG-conjugates play a significant role in the accelerated blood clearance (ABC) phenomenon. *Journal of Controlled Release*, *165*, 183–190.

Silva, G. A., Ducheyne, P., & Reis, R. L. (2007). Materials in particulate form for tissue engineering. 1. Basic concepts. *Journal of Tissue Engineering and Regenerative Medicine*, *1*, 4–24.

Son, S., Kim, G., Singha, K., Park, S., Ree, M., & Kim, W. J. (2011). Artificial cell membrane-mimicking nanostructure facilitates efficient gene delivery through fusogenic interaction with the plasma membrane of living cells. *Small*, *7*, 2991–2997.

Swain, S. K., & Sarkar, D. (2013). Study of BSA protein adsorption/release on hydroxyapatite nanoparticles. *Applied Surface Science*, *286*, 99–103.

Wang, F. H., Zhang, D. R., Duan, C. X., Jia, L. J., Feng, F. F., & Zhang, Q. (2011). Preparation and characterizations of a novel deoxycholic acid-O-carboxymethylated chitosan–folic acid conjugates and self-aggregates. *Carbohydrate Polymers*, *84*, 1192–1200.

Wang, Z. H., Zeng, R., Tu, M., & Zhao, J. H. (2012). A novel biomimetic chitosan-based nanocarrier with suppressing non-specific protein interactions. *Materials Letters*, *77*, 38–40.

Wu, M. M., Guo, K., Dong, H. W., Zeng, R., Tu, M., & Zhao, J. H. (2014). In vitro drug release and biological evaluation of biomimetic polymeric micelles self-assembled from amphiphilic deoxycholic acid–phosphorylcholine–chitosan conjugate. *Materials Science and Engineering: C*, *45*, 162–169.

Yoo, J. W., Irvine, D. J., Discher, D. E., & Mitragotri, S. (2011). Bio-inspired, bioengineered and biomimetic drug delivery carriers. *Nature Reviews Drug Discovery*, *10*, 521–535.

Zeng, R., Guo, K., Wang, Z. H., Tu, M., Zhao, J. H., & Wang, J. (2012). Synthesis and self-assembly of biomimetic phosphorylcholine-bound chitosan derivatives. *Reactive & Functional Polymers*, *72*, 745–751.

Zhou, W. B., Liu, X. S., & Ji, J. (2012). Fast and selective cancer cell uptake of therapeutic gold nanorods by surface modifications with phosphorylcholine and Tat. *Journal of Materials Chemistry*, *22*, 13969–13976.